

**This item is the archived peer-reviewed author-version of:**

Synergetic enhancement of quantum yield and exciton lifetime of monolayer WS<sub>2</sub> by proximal metal plate and negative electric bias

**Reference:**

Tran Trang Thu, Lee Yongjun, Roy Shrawan, Tran Thi Uyen, Kim Youngbum, Taniguchi Takashi, Watanabe Kenji, Milošević Milorad, Lim Seong Chu, Chaves Andrey, ....- Synergetic enhancement of quantum yield and exciton lifetime of monolayer WS<sub>2</sub> by proximal metal plate and negative electric bias  
ACS nano - ISSN 1936-086X - 18:1(2023), p. 220-228  
Full text (Publisher's DOI): <https://doi.org/10.1021/ACSNANO.3C05667>  
To cite this reference: <https://hdl.handle.net/10067/2028110151162165141>

# **Synergetic enhancement of quantum yield and exciton lifetime of monolayer WS<sub>2</sub> by proximal metal plate and negative electric bias**

Trang Thu Tran<sup>1</sup>, Yongjun Lee<sup>1</sup>, Shrawan Roy<sup>1</sup>, Thi Uyen Tran<sup>2</sup>, Youngbum Kim<sup>1</sup>, Takashi Taniguchi<sup>3</sup>, Kenji Watanabe<sup>4</sup>, Milorad V. Milosevic<sup>5</sup>, Seong Chu Lim<sup>1,2</sup>, Andrey Chaves<sup>5,6\*</sup>, Joon I. Jang<sup>7,\*</sup>, and Jeongyong Kim<sup>1,\*</sup>

<sup>1</sup>Department of Energy Science, Sungkyunkwan University, Suwon 16419, Republic of Korea

<sup>2</sup>Department of Smart Fab Technology, Sungkyunkwan University, Suwon 16419, Republic of Korea

<sup>3</sup>International Center for Materials Nanoarchitectonics, National Institute for Materials Science, 1-1 Namiki, Tsukuba 305-0044, Japan

<sup>4</sup>Research Center for Functional Materials, National Institute for Materials Science, 1-1 Namiki, Tsukuba 305-0044, Japan

<sup>5</sup>Department of Physics, University of Antwerp, Groenenborgerlaan 171, B-2020, Antwerp, Belgium

<sup>6</sup>Departamento de Física, Universidade Federal do Ceará, Campus do Pici, CP 6030, CEP 60455-900, Fortaleza, Ceará, Brazil

<sup>7</sup>Department of Physics, Sogang University, Seoul 04107, Republic of Korea

## **Corresponding Authors**

\*A. C. (andrey@fisica.ufc.br); \*J. I. J. (jjcoupling@sogang.ac.kr); J. K. (j.kim@skku.edu)

**Abstract:** The efficiency of light emission is a critical performance factor of monolayer transition metal dichalcogenides (1L-TMDs) for photonic applications. While various methods to compensate lattice defects to improve the quantum yield (QY) of 1L-TMDs have been studied, exciton-exciton annihilation (EEA) is still the major nonradiative decay channel of excitons at high exciton densities. Here we demonstrate that combined use of proximal Au plate and negative electric gate bias (NEGB) for 1L-WS<sub>2</sub> provides the dramatic enhancement of the exciton lifetime at high exciton densities with the corresponding QY enhanced by 30 times and the EEA rate constant decreased by 80 times. Suppression of EEA by NEGB is attributed to the reduction of defect-assisted EEA process, which was then explained by our theoretical model. Our results provide a synergetic solution to cope with EEA to realize the high-intensity 2D light emitters using TMDs.

**Keywords:** WS<sub>2</sub>, two dimensional semiconductors, exciton-exciton annihilation, quantum yield, monolayer transition metal dichalcogenide, back gate bias, exciton lifetime

## Introduction

Light-emitting semiconductors in quantum dimension offer the advantages of tunable photon energy, high efficiency, and color purity, etc.<sup>1-8</sup>. Among them, two-dimensional (2D) transition metal dichalcogenides (TMDs) are semiconductors with direct bandgap in monolayer ranging from visible to near-infrared regime, which is an ideal quantum platform to develop exciton-based light-emitting devices<sup>7,9-12</sup>. The quantum yield (QY), the measure of the light-emission efficiency vs. absorption, is one of the most significant performance parameters of semiconductors for application as light-emitting diodes (LEDs). However, 1L-TMDs generally suffer from the high density of lattice defects. As a result, the QY values of 1L-TMDs, exfoliated or CVD-grown, have been reported to be very low<sup>12-16</sup>. Numerous methods of post-treatment using chemicals or electric bias have been reported to increase the photoluminescence (PL) of 1L-TMDs, and some of them were claimed to achieve near-unity QYs<sup>17-22</sup>. While the reliability of the measurement of the QY needs to be confirmed, the QY must be improved for achieving 1L-TMDs as practical devices.

Another serious challenge in achieving a high QY of 1L-TMDs is how to handle strong exciton-exciton interaction that usually ends up with a nonradiative Auger process, called exciton-exciton annihilation (EEA), of which probability increases steeply with increasing the exciton density ( $n_{ex}$ ). For high-quality 1L-TMDs with low defect densities, a significant drop in QY and PL lifetime by two orders of magnitude is routinely observed as  $n_{ex}$  increases<sup>21-24</sup>. Thus, EEA is the main factor limiting the quantum efficiency of LEDs based on TMDs, and without solving this problem the light intensity that can be extracted from 1L-TMDs will be limited to an impractical level. While the EEA processes in 1L-TMDs were studied extensively<sup>16,25-28</sup>, the active control or suppression of EEA has been relatively rare. Some examples include laser irradiation, hBN dielectric environment and plasma treatment, which were

reported to be effective in suppressing EEA <sup>24,29–32</sup>, and applying in-plane strain was found to be effective to keep the high QY in the high  $n_{ex}$  regime <sup>22,33</sup>. The enhancement of the QY was also achieved by implementing metal plate under 1L-TMDs, where exciton-exciton interaction was screened to suppress the EEA efficiency <sup>34</sup>.

On the other hand, owing to the atomically thin thickness of 2D TMDs, electric gate bias can significantly affect the PL properties of these materials <sup>21,35</sup>. The immediate role of gate bias is modulating the charge density and, consequently, the relative population of exciton complexes such as neutral excitons, trions and biexcitons etc, which directly affects the QY of 1L-TMDs <sup>21,36,37</sup>. It was previously shown that simple negative gate bias on 1L-MoS<sub>2</sub> or 1L-WS<sub>2</sub> could greatly increase the QY at low exciton densities, but the severe decrease of the QY still occurred with increasing exciton density because of strong EEA contribution <sup>21</sup>. Gate bias has also been used to control the energy of interlayer excitons of heterostacked bilayers of 1L-TMDs <sup>38,39</sup> via Stark effect. However, the exciton dynamics influenced by the electric field under gate bias was rarely studied. Sharma et al. <sup>40</sup> demonstrated that gate bias modulates the exciton lifetime and diffusion of 1L-WS<sub>2</sub>. It has also been demonstrated <sup>21,40</sup> that defects can be effectively passivated by such vertical bias, which emerges as an alternative to defect passivation techniques based on chemical treatment <sup>18–20</sup>. However, a proper systematic study on the effect of electric field by back-gate bias on exciton-exciton interaction or EEA has not been carried out in terms of the overall QY, especially at high exciton densities.

In this study, we show that applying negative electric gate bias (NEGB) to 1L-WS<sub>2</sub> on hBN/Au substrate causes the synergetic effect of suppressing EEA, leading to significantly enhanced QY and prolonged exciton lifetime at high exciton densities. While the metal substrate reduces typical exciton-exciton interaction by Coulomb screening, electrical passivation of defects by NEGB is crucial for further suppressing defect-assisted EEA to

systematically maximize QY and exciton lifetime. With the combined use of proximal metal substrate and back-gate bias, the QY was enhanced by 30 times, the EEA rate constant was reduced by 80 times and the exciton lifetime of 1.08 ns was achieved, the longest ever reported for 1L-WS<sub>2</sub> at  $n_{ex} = 1.5 \times 10^{11} \text{ cm}^{-2}$ . Our experimental results were also explained by a theoretical model that captures the essence of reducing defect-assisted EEA by out-of-plane electric field. Our result of mitigating EEA by electric field under proximal metal contact provides an advanced concept for controlling Coulomb interaction aiming at high-intensity light emission in 1L-TMDs.

## Results and Discussion

Figure 1a shows the schematics of sample configurations, where 1L-WS<sub>2</sub> was prepared on 300-nm-thick SiO<sub>2</sub> on the Si substrate or on 8-nm-thick hBN on the deposited Au film (50 nm in thickness) on the SiO<sub>2</sub>/Si substrate, which are denoted by Sample A and Sample B, respectively. Each sample was grounded by the top Au electrode to apply NEGB ( $V_g$ ). The corresponding optical microscopic views, PL intensity maps and atomic force microscopy (AFM) images of the samples are provided in Figs. S1–S4. Figure 1b shows the normalized PL spectra of Sample A at  $V_g = 0 \text{ V}$  (left panel) and at  $V_g = -20 \text{ V}$  (right panel) for varying excitation powers ranging from 0.27 to 14900 nW, which correspond to generation rates of excitons ranging from  $5.6 \times 10^{15}$  to  $3.1 \times 10^{20} \text{ cm}^{-2}\text{s}^{-1}$ ; See the Supporting Information for the calculation of the generation rate. The observed PL peak at 2.02 eV of 1L-WS<sub>2</sub> is in good agreement with previous results<sup>12,23</sup>. The PL spectra are composed of mostly neutral excitons, as the deconvolution fitting indicates that the spectral ratios of excitons and trions are 94 % and 6 %, respectively, suggesting a very low initial charge (electron) density of our exfoliated 1L-WS<sub>2</sub>. The spectral ratio of trions was further reduced to 4 % by applying NEGB due to

electric passivation of sulfur vacancies and depletion of excess electrons<sup>40–42</sup>. We note that the PL spectral shape remained almost the same throughout the four orders of magnitude when varying the excitation power from 0.27 to 674 nW beyond which the spectral weight of trions slightly increased.

In Fig. 1c, we show the normalized PL spectra of Sample B with the excitation power ranging from 0.27 to 14900 nW (from  $5.1 \times 10^{15}$  to  $2.8 \times 10^{20} \text{ cm}^{-2}\text{s}^{-1}$  in generation rate) at  $V_g = 0 \text{ V}$  (left panel) and at  $V_g = -5 \text{ V}$  (right panel). The PL peak at 1.99 eV is slightly lower than that observed from Sample A, possibly due to different dielectric environment and strain induced from the transfer procedure<sup>25,43–47</sup>. Without NEGB, spectral ratios of excitons and trions were 97 % and 3 %, respectively, whereas virtually no trion portion was detected with NEGB, indicating that the combined use of Au substrate and NEGB completely depleted excess electrons. Indeed, the PL curves in the right panel of Fig. 1c keep the same shape throughout the whole excitation range.

The presence of proximal metal plate or NEGB critically affects the exciton dynamics. In Fig. 2a, we display the representative PL decay curves obtained from time-resolved PL (TRPL) measurement of Sample A at  $V_g = 0 \text{ V}$  (left panel) and at  $V_g = -20 \text{ V}$  (right panel). TRPL was conducted at the initial exciton density ( $n_{ex}(0)$ ) varying from  $3.6 \times 10^8$  to  $1.5 \times 10^{11} \text{ cm}^{-2}$ , where  $n_{ex}(0)$  was estimated for each pump fluence (from  $3.2 \times 10^{-3}$  to  $1.4 \mu\text{Jcm}^{-2}$ ) based on the calculated absorption for the multilayer substrate structure<sup>25,34,48</sup>; see the Supporting Information. We note the gradual decrease of the exciton lifetime with increasing  $n_{ex}(0)$ , which is typical of EEA in 1L-TMDs. In order to examine the impact of NEGB on this process, we applied  $V_g = -20 \text{ V}$ , which resulted in PL decay being notably slower at the low  $n_{ex}(0)$  regime due to defect passivation by excess charge depletion<sup>21</sup>. However, the decay rate gradually increases again with increasing pump fluence, indicating

that EEA is still active under NEGB.

When EEA comes into play, the temporal behavior of excitons is no longer properly explained by a simple exponential decay. For the quantitative analysis, the mean lifetime ( $\tau_{ave}$ ) for a given TRPL data was estimated at time when the PL intensity becomes  $1/e$  of the PL intensity at  $t = 0$ . The resulting  $\tau_{ave}$  is plotted as a function of  $n_{ex}(0)$  in Fig. 2c. Typically,  $\tau_{ave}$  of 1L-TMDs at a low  $n_{ex}$  is determined by the sample condition such as defect density and doping states<sup>11,23,29</sup>. In general, a sample with a low defect density and a low excess charge density shows a long  $\tau_{ave}$  value of several nanoseconds<sup>20,23,49</sup>. In Sample A,  $\tau_{ave}$  is a constant below  $10^8 \text{ cm}^{-2}$  as shown in Figs. S5a and S10c. However, it tends to exhibit a significant reduction of  $\tau_{ave}$  with increasing  $n_{ex}(0)$ , because EEA becomes dominant over the exciton trapping process by defects. Thus, at  $n_{ex}$  beyond  $10^{11} \text{ cm}^{-2}$ , the  $\tau_{ave}$  value of a high-quality sample is limited to the range of a few hundred picoseconds or less.

At the lowest  $n_{ex} = 3.6 \times 10^8 \text{ cm}^{-2}$ , we note that  $\tau_{ave}$  increases from 570 ps without NEGB to 1.34 ns with NEGB, clearly indicating the effect of defect passivation. With increasing  $n_{ex}(0)$ ,  $\tau_{ave}$  gradually reduces because of EEA. However, the apparent “slope” of decreasing  $\tau_{ave}$  with increasing  $n_{ex}$  is steeper under NEGB, so that, at very high densities above  $1 \times 10^{11} \text{ cm}^{-2}$ , the lifetime of the biased sample approaches  $\tau_{ave}$  obtained without NEGB: See also Fig. S5 obtained from an additional Sample A. This effect arises from electrical passivation of defects in 1L-WS<sub>2</sub> under NEGB in which excitons may undergo more efficient diffusion, causing more frequent EEA in reducing the exciton lifetime<sup>21,22</sup>. This persistent contribution of EEA to lowering the QY suggests that strong PL emission at high exciton densities requires not only passivation of defects, but also suppression of the remaining EEA channels, which is the main purpose of adding a metallic (Au) substrate to the sample with NEGB as illustrated in the right panel of Fig. 2b.

The left and right panels of Fig. 2b show the PL decay curves of Sample B with  $n_{ex}(0)$  varying from  $1.7 \times 10^8$  to  $1.5 \times 10^{11} \text{ cm}^{-2}$  (from  $1.5 \times 10^{-3}$  to  $1.3 \text{ }\mu\text{Jcm}^{-2}$ ) without and with NEGB, respectively. Although hBN encapsulation is known to decrease the PL lifetime due to exciton delocalization<sup>32,50</sup>, this is not the case with the metal proximity effect<sup>34</sup>, leading to an increase of  $\tau_{ave}$  at  $n_{ex}(0) \approx 10^8 \text{ cm}^{-2}$  from 570 ps in Sample A to 740 ps in Sample B. Furthermore,  $\tau_{ave}$  of Sample B was significantly enhanced at high exciton densities, because of the suppression of EEA via metal-induced screening of dipolar exciton fields<sup>34</sup>. Quite intriguingly, this affirmative effect is much more pronounced with NEGB. For instance,  $\tau_{ave}$  of Sample B displays a long lifetime of 1.08 ns even at  $n_{ex}(0) = 2 \times 10^{11} \text{ cm}^{-2}$ , which is slightly reduced from the value of 2.09 ns at  $n_{ex}(0) < 10^{10} \text{ cm}^{-2}$ . This is in a sharp contrast to the steep reduction from 1.34 ns to 190 ps under NEGB observed in Sample A over the similar  $n_{ex}(0)$  range. Clearly, the effect of NEGB is much more evident for Sample B. In fact, distinct EEA effects in Sample A and Sample B are also well evidenced by monitoring the corresponding spatial profiles of the PL as shown in Fig. S6, which exhibits a notably broader PL profile for Sample A via more exciton diffusion and Auger broadening<sup>26</sup>, compared with Sample B. We emphasize that the observed  $\tau_{ave}$  of 1.08 ns at  $n_{ex}(0) = 1.5 \times 10^{11} \text{ cm}^{-2}$  is the longest reported so far for 1L-WS<sub>2</sub> as shown in Fig. S7, indicating the effectiveness of the synergetic usage of proximal metal plate and NEGB for enhancing the exciton lifetime.

The TRPL measurement provides the direct measure of the time-varying density of photoexcited excitons in 1L-TMDs<sup>23,34,51</sup>. At low excitation levels, the main decay channel of excitons is recombination at structural defects<sup>51</sup>, which can be fit by a single exponential function<sup>12</sup>. As  $n_{ex}$  increases, however, EEA starts to act as the main decay channel for excitons. The contribution of defects and EEA to  $n_{ex}(t)$  can be described by the rate equation<sup>50</sup>,

$$\frac{dn_{ex}(t)}{dt} = \frac{-n_{ex}(t)}{\tau_0} - \gamma n_{ex}(t)^2, \quad (1)$$

where  $n_{ex}$  is the exciton density,  $\tau_0$  is the PL lifetime measured at the lowest exciton density, and  $\gamma$  is the EEA rate constant. The solution to Eq. (1) can be simplified to  $n_{ex}(t) = (\gamma\tau_0)^{-1}exp(-t/\tau_0)$  at high densities, which is fitted against the TRPL traces to extract  $\gamma$ <sup>34</sup>.

In Fig. 3a, we plot  $\gamma$  estimated for Sample A and Sample B. Results of multiple samples with the same substrate configuration are shown as separate data points and the error bar represents the standard deviation of  $\gamma$  estimated from the TRPL curves of different initial exciton densities (pump fluences) for the same sample. All samples displayed the reduction of  $\gamma$  with NEGB, which was only a factor of 2 to 4 for Sample A, but it reduces by a factor of  $\sim 9$  in Sample B. Compared to the average of  $\gamma$  ( $0.4637 \text{ cm}^{-2}\text{s}^{-1}$ ) obtained from two batches of Sample A without NEGB (two open circles in Fig. 3a), the measured  $\gamma$  value ( $0.00574 \text{ cm}^{-2}\text{s}^{-1}$ ) is 80 times smaller in Sample B with NEGB (red dot in Fig. 3a). We previously reported the effect of suppressing EEA by an order of magnitude in  $\gamma$  by using a metal substrate<sup>34</sup>. Here, we demonstrate that another order of magnitude of reduction in  $\gamma$  was achieved with NEGB, showing the synergetic combination of metal proximity and NEGB to suppress EEA in 1L-TMDs. In order to confirm the reproducibility of our results, we performed the TRPL measurements on additional two samples in the Sample B configuration with 17-nm-thick hBN. The corresponding TRPL data and plots of  $\tau_{ave}$  vs. exciton density are provided in Fig. S8 with and without NEGB. Significant drops in the estimated  $\gamma$  is also shown in Fig. S9, indicating effective suppression of EEA by combined use of proximal metal screening and NEGB<sup>33</sup>. Furthermore, we also conducted the similar measurements using different batches of exfoliated 1L-WS<sub>2</sub> and consistently observed reduction in  $\gamma$  by two orders of magnitude when using a metal substrate with NEGB as demonstrated by Figs. S10 and S11.

We conducted the field-effect transistor (FET) measurement on Sample B as shown in Fig. 3b: See Figs. S12 and S13 for the images of the FET device and the transfer results from

a device on the SiO<sub>2</sub>/Si substrate. It showed the typical n-type transfer characteristics, where the electron mobility of  $3.48 \text{ cm}^2\text{V}^{-1}\text{s}^{-1}$  is estimated under positive gate bias with the ON/OFF ratio of  $2.2 \times 10^3$ , and these values are consistent with the previous reports<sup>52,53</sup>. With NEGB increasing up to  $-6 \text{ V}$ , the OFF-state was maintained, confirming that no hole charges were induced. Therefore, we rule out any possibility that induced holes are responsible for reduced EEA through charge screening of exciton-exciton interaction. Noticeably, the threshold voltage was estimated to be nearly  $0 \text{ V}$ , confirming the minimal level of intrinsic excess charges (electrons) of our 1L-WS<sub>2</sub>, consistent with the exciton-dominant PL spectra from Sample B (Fig. 1c). All these observations confirm that our 1L-WS<sub>2</sub> samples are intrinsically very low in excess charges and the charge density remains constant under NEGB. Since the Fermi level of 1L-WS<sub>2</sub> lies within the bandgap and the work function of contact metal Au, we believe that the hole charges are mostly accumulated near the contact without being injected into the 1L-WS<sub>2</sub> area<sup>54</sup>.

Another possible effect expected for such a biased system is vertical polarization of excitons. However, this effect is not relevant, since the monolayer thickness is too thin to produce significant dipolar effects. Indeed, a hallmark signature of dipolar excitons (e.g. in van der Waals heterobilayers) is the blueshift of the exciton peak with increasing the exciton density due to dipolar exciton-exciton interaction<sup>55</sup>. This effect is not observed in our experimental results, thus confirming that any vertical polarization of excitons must be weak in our system. Therefore, the most significant effect of the bias in our samples is passivation of defects. We thus explain the origin of reduced EEA, especially in samples with strong dielectric screening due to the presence of Au, by electric passivation of defects, which suppresses not only the defect capture of electrons, but also defect-assisted EEA processes.

Three types of nonradiative scattering events experienced by excitons in 1L-TMDs are

schematically illustrated in Fig. 3c. In the defect-assisted exciton scattering process (process I), the scattered electron from an initial exciton is trapped in a defect, while the energy lost by the electron is transferred to a hole, thus hindering PL. In principle, a similar process may occur for holes, but this is much less probable because defects from S vacancies in 1L-WS<sub>2</sub> have an energy  $E_d$  close to (far from) the conduction (valence) band edge, thus making WS<sub>2</sub> effectively n-doped<sup>56</sup>. Process II corresponds to typical EEA, in which electron-electron scattering induces recombination of one exciton, but the recombination energy is transferred to the second electron in a Meitner-Auger process, thus resulting in an unbound electron-hole pair in the final state. In our previous report<sup>34</sup>, we argued that electron-electron interactions are responsible for the leading contribution to nonradiative EEA in 1L-TMDs, and that this interaction could be screened by a proximate metal. Process III is defect-assisted EEA where the scattered electron fills the defect state, transferring energy to the electron of the second exciton. This process is qualitatively analyzed here within the same model in order to predict the effect of bias-induced defect passivation on EEA.

Process I occurs with a rate approximately given by  $R_D \approx \tau_D^{-1} \propto \alpha_D |\chi_D(q_D)|^2 |\Phi_{1s}(r=0)|^2 V_D(q_D)^2$ , where  $R_D$  represents the rate of exciton decay due to trapping by defects,  $\tau_D$  is the corresponding average time,  $\Phi_{1s}(0)$  is the ground-state exciton wave function at the relative coordinate  $r = 0$ ,  $V_D(q_D)$  and  $\chi_D(q_D)$  are the electron-defect interaction potential and the defect state wave function at the relative exciton wavevector  $q_D$  (see the Supporting Information)<sup>57</sup>, respectively, and  $\alpha_D = n_D(1 - f_D)$  is the effective density of active defects, i.e., the fraction of the total density of defects  $n_D$  that is not passivated. External bias is expected to increase the fraction of passivated defects  $f_D$  and, consequently, the exciton lifetime. The screening due to the metal proximity is also expected to affect  $V_D(q_D)$  and  $\Phi_{1s}(0)$ , thus increasing the lifetime even further. This process does not depend on the exciton density.

Process II has been discussed in details in Ref. <sup>34</sup>– the rate at which this process occurs is given by  $R_{EEA} = \gamma_{EEA} n_{ex} \propto \sum_{\vec{K}_1, \vec{K}_2} |M_{EEA}(\vec{K}_1, \vec{K}_2, \vec{K}_f, \vec{k}_f)|^2 n_{ex}$ , where the sum is made over different values of momenta  $\vec{K}_1$  and  $\vec{K}_2$  of the initial pair of excitons, and the scattering matrix  $M_{EEA} = \langle i|V|f\rangle$  involves the screened electron-electron interaction potential  $V(K)$  <sup>58</sup>, an initial state  $|i\rangle = |X_1\rangle|X_2\rangle$  composed of two excitons, and a final state  $|f\rangle = |\vec{k}_e \vec{k}_h\rangle$  composed of an unbound electron and hole pair, whose momenta are  $\vec{k}_e$  and  $\vec{k}_h$ , respectively. While the bias barely affects  $R_{EEA}$ , the screening due to proximity with a metal significantly decreases  $V(K)$  and affects  $\Phi_{1s}(0)$  as well, thus reducing the EEA rate ( $\gamma_{EEA}$ ) in process II by one order of magnitude in Sample B <sup>34</sup>.

Process III is modeled in a way that is similar to processes I and II, but the exact form of the corresponding scattering matrix is cumbersome <sup>15</sup>. We simplify the discussion by considering that the rate for this process must be represented by  $R_{D-EEA} = \gamma_{D-EEA} n_{ex} \propto \alpha_D |\Phi_{1s}(r=0)|^2 |\Phi_{1s}(q_D)|^6 |\chi_D(q_D)|^2 |V(q_D)|^2 n_{ex}$ . The approximations involved in this expression are discussed in the Supporting Information. Therefore,  $R_{D-EEA}$  is clearly affected by electric defect passivation, via  $\alpha_D$ , and by the proximity with a metal, via screened interaction potentials and the modified exciton wave function.

Considering processes I–III, Eq. (1) can be expressed by

$$\frac{dn_{ex}}{dt} = -\left(\frac{1}{\tau_r} + \frac{1}{\tau_D}\right) n_{ex} - (\gamma_{EEA} + \gamma_{D-EEA}) n_{ex}^2, \quad (2)$$

where  $\frac{1}{\tau_0} = \frac{1}{\tau_r} + \frac{1}{\tau_D}$  and  $\gamma = \gamma_{EEA} + \gamma_{D-EEA}$ . In the presence of bias, the low-density lifetime in Fig. 2c for Sample A increases by a factor of 2.35. The bias is only expected to affect  $\alpha_D$ , and therefore, this increase in  $\tau_{ave}$  must result from bias-induced passivation of the defects. However, the lifetime in this case is strongly dependent on  $n_{ex}(0)$ , indicating that processes II and III are still active. In proximity with a metal (Sample B), at low densities under no NEGB,

the lifetimes in Fig. 2d slightly increase as compared to those in Fig. 2c, because of the screening effect on  $V_D(q_D)$  and  $\Phi_{1s}(r)$  in  $R_D$ . In this case, the lifetime is less affected by the exciton density and exhibits significant reduction for  $n_{ex}(0) > 10^{10} \text{ cm}^{-2}$ , as a result of the suppression of  $\gamma_{EEA}$ <sup>34</sup>. Finally, in the presence of bias,  $\gamma_{D-EEA}$  is also suppressed and the exciton lifetime in Fig. 2d is not only longer, but also almost independent of  $n_{ex}(0)$  up to  $n_{ex}(0) \approx 10^{11} \text{ cm}^{-2}$ .

Using the analytical solution to Eq. (2), the average lifetime is calculated by

$$\tau_{ave} = \tau_0 \ln \left( \frac{e + \gamma n_{ex}(0) \tau_0}{1 + \gamma n_{ex}(0) \tau_0} \right), \quad (3)$$

where the radiative lifetime<sup>59</sup> is estimated as  $\tau_r = \frac{3k_B T}{2E_0} \frac{4\pi\hbar\varepsilon}{k_0} \left( \frac{E_X a_B}{\hbar v} \right)^2$ , where  $k_B$  is the Boltzmann constant,  $T$  is the temperature,  $a_B$  is the exciton Bohr radius,  $\varepsilon = 11.74\varepsilon_0$  is the effective dielectric constant of 1L-WS<sub>2</sub><sup>58</sup>,  $E_X$  is the exciton energy, and  $E_0 = \hbar^2 k_0^2 / 2 (m_e + m_h)$  is the exciton kinetic energy at the light wavevector  $k_0 = E_X \sqrt{\varepsilon} / \hbar c$ . The Kane velocity is calculated as  $v = \sqrt{E_g / 2 m_e}$ , where  $E_g$  is the quasiparticle gap and the electron and hole effective masses are  $m_e \approx m_h = 0.34m_0$ . At room temperature, this expression leads to  $\tau_r = 4.42 \text{ ns}$  for 1L-WS<sub>2</sub> on SiO<sub>2</sub> without a metal substrate. In the presence of defects, the calculated lifetime  $\tau_0$  is about 0.7 ns using  $\frac{1}{\tau_0} = \frac{1}{\tau_r} + \frac{1}{\tau_D}$  with a typical value of  $n_D = 5 \times 10^{12} \text{ cm}^{-2}$ <sup>14,60,61</sup>. Note that this value is similar to the experimentally observed lifetime ( $\tau_{ave}$ ) in Fig. 2c at low exciton densities without electric bias. In this case,  $\gamma$  is dominated by  $\gamma_{EEA}$ , and therefore, the effect of defect passivation in EEA is not significant.

Figures 4a and 4b show the theoretical prediction for  $\tau_{ave}$  obtained from Eq. (3) for vacuum/1L-WS<sub>2</sub>/SiO<sub>2</sub> (Sample A) and 1L-WS<sub>2</sub>/hBN/Au (Sample B), respectively, assuming two different values for the fraction of passivated defects, which mimics the effect of increasing bias. Details of the parameters in the theoretical model are provided in the SI. Note that  $\tau_{ave}$  is

a constant in the low density regime for the two sample configurations, but it undergoes gradual decrease as the exciton density increases. As the density of active defects  $\alpha_D$  decreases,  $\tau_{ave}$  increases at low densities. In the high-density regime, however, the increase in  $\tau_{ave}$  is much less significant, which is in a qualitative agreement with Fig. 2c. In Sample B, metal screening lowers  $\gamma_{EEA}$  (process II) by an order of magnitude<sup>34</sup>. In this case, the EEA rate constant is dominated by  $\gamma_{D-EEA}$ , which depends on the bias. Indeed, Fig. 4b shows that  $\tau_{ave}$  is less dependent on the initial exciton density  $n_{ex}(0)$  as compared to Fig. 4a, even at zero bias. As the fraction of passivated defects increases,  $\tau_{ave}$  becomes even less dependent on  $n_{ex}(0)$ , in a good agreement with the experimental results shown in Fig. 2d. Therefore, our theoretical model emphasizes that defect-assisted EEA should be suppressed using the metal substrate under electric bias for maximizing the QY of 1L-WS<sub>2</sub>.

Clearly, prolonged lifetime and reduced EEA lead to the enhancement of the QY. In Fig. 5, we show QY vs. exciton generation rate ( $G$ ) for Sample A and Sample B with and without NEGB: QY vs.  $G$  and PL spectra of other samples are provided in Figs. S5b, S14, S15 and S16: Details for the QY measurement of 1L-WS<sub>2</sub> are described in the Supporting Information. At low exciton densities under NEGB, the QY of both samples showed a slight increase due to the depletion of excess charges<sup>20</sup> and electrostatic defect passivation<sup>21,36,62</sup>, which is in line with our theoretical model. Upon increasing  $G$ , the threshold  $G$  values for the QY drop are higher for Sample B than Sample A and with NEGB than without NEGB; lowest at  $2 \times 10^{15} \text{ cm}^{-2}\text{s}^{-1}$  for Sample A without NEGB and highest at  $1 \times 10^{17} \text{ cm}^{-2}\text{s}^{-1}$  for Sample B with NEGB. Furthermore, the slope of decreasing QY with increasing  $G$  is smallest for Sample B with NEGB. The corresponding QY at  $\sim 2 \times 10^{20} \text{ cm}^{-2}\text{s}^{-1}$  is calculated to 4.8 %, which is 30 times higher than 0.17 % for Sample A without NEGB. The PL spectra normalized with their respective QYs at  $\sim 2 \times 10^{20} \text{ cm}^{-2}\text{s}^{-1}$  (right panels) visually manifest the

synergetic effect of proximate metal and NEGB.

## Conclusion

In summary, we have demonstrated that combined use of hBN/Au substrate and back-gate bias can greatly suppress exciton-exciton interactions in 1L-WS<sub>2</sub>, thereby enhancing the QY by 30 times and reducing the EEA rate by 80 times, compared to the samples on typical SiO<sub>2</sub> substrates. Our theoretical model clarifies the roles of the metal plate and electric bias for screening Coulomb interactions and suppressing defect-mediated EEA, respectively. Consequently, the longest exciton lifetime of 1.08 ns was achieved at  $n_{ex} = 1.5 \times 10^{11} \text{ cm}^{-2}$  in 1L-WS<sub>2</sub>. Our combined theoretical and experimental study provides an effective but simple access to greatly suppressing the QY-deteriorating exciton-exciton interactions in 1L-TMDs through the synergetic solution for high-performance 2D light-emitters based on TMDs and potentially other emerging 2D semiconducting materials.

## **Experimental Methods**

### **Sample preparation**

The fabrication process was started with mechanical exfoliation of bulk WS<sub>2</sub> (HQ Graphene) and hBNs (National Institute for Materials Science, Japan) on top of polydimethylsiloxane (PDMS). Monolayer samples were identified by optical contrast. The thickness of hBN was about from 5 to 20 nm, which was first verified by optical microscope and then confirmed using atomic force microscopy (XE-120, Park Systems). E-beam lithography was used to define the contact pattern on the Si substrate covered by 300-nm-thick SiO<sub>2</sub>. The top contact metal Au (50 nm) was deposited immediately after e-beam lithography. Heterostructures were assembled via a dry peel/lift technique on gold contacts<sup>34,63,64</sup>. For samples on the hBN/Au, the top hBN layer (9 nm thickness) was capped to prevent sample degradation by ambient oxidation, which was found to be more severe than Sample A, probably due to the higher electrostatic attraction of Au toward ambient air molecules such as oxygen and water. For each transferred layer, samples were annealed at 80°C in the vacuum oven for 2 hours, because this process helps to remove the possible residue from PDMS and increases interlayer binding between WS<sub>2</sub> and hBN in the heterostructures. The monolayers were electrically grounded by the Au source contact, and the back-gate voltage was applied to the Si substrate or hBN/Au.

### **Electrical and Optical Measurement**

Electric bias was applied to the device by a source measurement unit (Keithley 6487), while the Au source contact was grounded. For PL measurements, confocal microscope (Alpha-300S, WITec Instrument GmbH) with a 100x objective lens ( $N.A. = 0.9$ ) and a frequency-doubled neodymium-doped yttrium aluminum garnet laser (532 nm CW excitation) was used. TRPL measurements were performed using the same microscope using a pulsed laser with an excitation wavelength of 488 nm (BDL-488, Becker & Hickl GmbH) and a repetition rate of

80 MHz, a high-speed hybrid detector (HPM-100-40, Becker & Hickl GmbH) and a time-correlated single-photon counting module (TCSPC, Becker & Hickl GmbH). All measurements reported were conducted at room temperature under an ambient environment.

### **Supporting Information**

The Supporting Information is available free of charge.

- Optical microscope views and PL immensity maps of samples; plots of PL lifetime and QY for additional sample sets; spatial profiles of PL with focused excitation depending on the substrate configuration; Comparison of PL lifetimes of 1L-WS<sub>2</sub> reported from previous works and this work; TRPL curves and EEA rate constants of additional sample sets; PL spectra with varying excitation powers and plot of QY vs. exciton generation rate for 1L-WS<sub>2</sub> on 17 nm hBN/Au and 11 nm hBN/Au substrates; electric transfer curves and microscope view for FET device on SiO<sub>2</sub> substrate; calibration of optical interference on the absorption and the PL intensity of 1L-WS<sub>2</sub> by multilayer substrates; Estimation details of the generation rate and the exciton density; details of theoretical approach for the density dependence of exciton lifetime; estimation details of absolute QY of 1L-WS<sub>2</sub>

### **Author contributions**

T.T.T. and Y.L. fabricated the samples, performed optical characterization, analyzed data. T.T.T. and T.U.T. performed electrical measurement. S.R. and Y.K. prepared the reference samples for QY measurement. T.T.T. and J.K. analyzed the data and wrote the manuscript. T.T. and K.W. synthesized and discussed the role of high-quality hBNs. J.I.J. analyzed the data and wrote the manuscript. A.C. and M.V.M. performed theoretical calculation and wrote the manuscript.

### **Notes**

The authors declare no competing financial interests.

## **Acknowledgements**

This work was supported by the Samsung Research Funding & Incubation Center of Samsung Electronics, under project no. SRFC-MA1802-02. J.K. acknowledges supports from National Research Foundation of Korea (NRF) funded by the Ministry of Education (2021R1A6A1A03039696; 2022R1A2C2009412; 2022K2A9A1A06093582) and the Commercialization Promotion Agency for R&D outcomes funded by the Ministry of Science and ICT (grant No:RS-2023-00243196). J.I.J. acknowledges the support of the Basic Science Research Programs (2020R1F1A1069646 and 2021R1A2C2013625) and the Basic Research Laboratory Program (2022R1A4A1033562) through the National Research Foundation of Korea (NRF), funded by the Korean government. A.C. acknowledges support from the Brazilian Research Council (CNPq), through the PQ and UNIVERSAL programs. M.V.M. and A.C. acknowledge support from the Research Foundation - Flanders (FWO). K.W. and T.T. acknowledge support from the Elemental Strategy Initiative conducted by the MEXT, Japan, (Grant Number JPMXP0112101001), JSPS KAKENHI (Grant Numbers 19H05790 and 21H05233) and A3 Foresight by JSPS.

## References

- (1) Zhang, X.; Qiao, X. F.; Shi, W.; Wu, J. Bin; Jiang, D. S.; Tan, P. H. Phonon and Raman Scattering of Two-Dimensional Transition Metal Dichalcogenides from Monolayer, Multilayer to Bulk Material. *Chem. Soc. Rev.* **2015**, *44* (9), 2757–2785. <https://doi.org/10.1039/c4cs00282b>.
- (2) Choi, W.; Choudhary, N.; Han, G. H.; Park, J.; Akinwande, D.; Lee, Y. H. Recent Development of Two-Dimensional Transition Metal Dichalcogenides and Their Applications. *Mater. Today* **2017**, *20* (3), 116–130. <https://doi.org/10.1016/j.mattod.2016.10.002>.
- (3) Sharbirin, A. S.; Roy, S.; Tran, T. T.; Akhtar, S.; Singh, J.; Duong, D. L.; Kim, J. Light-Emitting Ti<sub>2</sub>N (MXene) Quantum Dots: Synthesis, Characterization and Theoretical Calculations. *J. Mater. Chem. C* **2022**, *10* (16), 6508–6514. <https://doi.org/10.1039/d2tc00568a>.
- (4) Tan, C.; Cao, X.; Wu, X. J.; He, Q.; Yang, J.; Zhang, X.; Chen, J.; Zhao, W.; Han, S.; Nam, G. H.; Sindoro, M.; Zhang, H. Recent Advances in Ultrathin Two-Dimensional Nanomaterials. *Chem. Rev.* **2017**, *117* (9), 6225–6331. <https://doi.org/10.1021/acs.chemrev.6b00558>.
- (5) Wang, Z.; Jingjing, Q.; Wang, X.; Zhang, Z.; Chen, Y.; Huang, X.; Huang, W. Two-Dimensional Light-Emitting Materials: Preparation, Properties and Applications. *Chem. Soc. Rev.* **2018**, *47* (16), 6128–6174. <https://doi.org/10.1039/c8cs00332g>.
- (6) Kim, H.; Beack, S.; Han, S.; Shin, M.; Lee, T.; Park, Y.; Kim, K. S.; Yetisen, A. K.; Yun, S. H.; Kwon, W.; Hahn, S. K. Multifunctional Photonic Nanomaterials for Diagnostic, Therapeutic, and Theranostic Applications. *Adv. Mater.* **2018**, *30* (10), 1–33. <https://doi.org/10.1002/adma.201701460>.

- (7) Wang, F.; Pei, K.; Li, Y.; Li, H.; Zhai, T. 2D Homojunctions for Electronics and Optoelectronics. *Adv. Mater.* **2021**, *33* (15), 2005303. <https://doi.org/10.1002/adma.202005303>.
- (8) Zhao, H.; Zhao, Y.; Song, Y.; Zhou, M.; Lv, W.; Tao, L.; Feng, Y.; Song, B.; Ma, Y.; Zhang, J.; Xiao, J.; Wang, Y.; Lien, D.-H.; Amani, M.; Kim, H.; Chen, X.; Wu, Z.; Ni, Z.; Wang, P.; Shi, Y.; Ma, H.; Zhang, X.; Xu, J.-B.; Troisi, A.; Javey, A.; Wang, X. Strong Optical Response and Light Emission from a Monolayer Molecular Crystal. *Nat. Commun.* **2019**, *10* (1), 5589. <https://doi.org/10.1038/s41467-019-13581-9>.
- (9) Shao, L.; Zhuo, X.; Wang, J. Advanced Plasmonic Materials for Dynamic Color Display. *Adv. Mater.* **2018**, *30* (16), 1704338. <https://doi.org/10.1002/adma.201704338>.
- (10) Choi, J.; Florian, M.; Steinhoff, A.; Erben, D.; Tran, K.; Kim, D. S.; Sun, L.; Quan, J.; Claassen, R.; Majumder, S.; Hollingsworth, J. A.; Taniguchi, T.; Watanabe, K.; Ueno, K.; Singh, A.; Moody, G.; Jahnke, F.; Li, X. Twist Angle-Dependent Interlayer Exciton Lifetimes in van Der Waals Heterostructures. *Phys. Rev. Lett.* **2021**, *126* (4), 47401. <https://doi.org/10.1103/PhysRevLett.126.047401>.
- (11) Pu, J.; Takenobu, T. Monolayer Transition Metal Dichalcogenides as Light Sources. *Adv. Mater.* **2018**, *30* (33), 1707627. <https://doi.org/10.1002/adma.201707627>.
- (12) Yuan, L.; Huang, L. Exciton Dynamics and Annihilation in WS<sub>2</sub> 2D Semiconductors. *Nanoscale* **2015**, *7* (16), 7402–7408. <https://doi.org/10.1039/C5NR00383K>.
- (13) Zhou, W.; Zou, X.; Najmaei, S.; Liu, Z.; Shi, Y.; Kong, J.; Lou, J.; Ajayan, P. M.; Yakobson, B. I.; Idrobo, J. C. Intrinsic Structural Defects in Monolayer Molybdenum Disulfide. *Nano Lett.* **2013**, *13* (6), 2615–2622. <https://doi.org/10.1021/nl4007479>.
- (14) Hong, J.; Hu, Z.; Probert, M.; Li, K.; Lv, D.; Yang, X.; Gu, L.; Mao, N.; Feng, Q.; Xie, L.; Zhang, J.; Wu, D.; Zhang, Z.; Jin, C.; Ji, W.; Zhang, X.; Yuan, J.; Zhang, Z. Exploring Atomic Defects in Molybdenum Disulphide Monolayers. *Nat. Commun.* **2015**,

- 6 (1), 6293. <https://doi.org/10.1038/ncomms7293>.
- (15) Wang, H.; Zhang, C.; Rana, F. Ultrafast Dynamics of Defect-Assisted Electron-Hole Recombination in Monolayer MoS<sub>2</sub>. *Nano Lett.* **2015**, *15* (1), 339–345. <https://doi.org/10.1021/nl503636c>.
- (16) Roy, S.; Sharbirin, A. S.; Lee, Y.; Kim, W. Bin; Kim, T. S.; Cho, K.; Kang, K.; Jung, H. S.; Kim, J. Measurement of Quantum Yields of Monolayer TMDs Using Dye-Dispersed PMMA Thin Films. *Nanomaterials* **2020**, *10* (6), 1032. <https://doi.org/10.3390/nano10061032>.
- (17) Neupane, G. P.; Tran, M. D.; Yun, S. J.; Kim, H.; Seo, C.; Lee, J.; Han, G. H.; Sood, A. K.; Kim, J. Simple Chemical Treatment to N-Dope Transition-Metal Dichalcogenides and Enhance the Optical and Electrical Characteristics. *ACS Appl. Mater. Interfaces* **2017**, *9* (13), 11950–11958. <https://doi.org/10.1021/acsami.6b15239>.
- (18) Roy, S.; Choi, W.; Jeon, S.; Kim, D. H.; Kim, H.; Yun, S. J.; Lee, Y.; Lee, J.; Kim, Y. M.; Kim, J. Atomic Observation of Filling Vacancies in Monolayer Transition Metal Sulfides by Chemically Sourced Sulfur Atoms. *Nano Lett.* **2018**, *18* (7), 4523–4530. <https://doi.org/10.1021/acs.nanolett.8b01714>.
- (19) Dhakal, K. P.; Roy, S.; Yun, S. J.; Ghimire, G.; Seo, C.; Kim, J. Heterogeneous Modulation of Exciton Emission in Triangular WS<sub>2</sub> Monolayers by Chemical Treatment. *J. Mater. Chem. C* **2017**, *5* (27), 6820–6827. <https://doi.org/10.1039/c7tc01833a>.
- (20) Amani, M.; Lien, D.-H.; Kiriya, D.; Xiao, J.; Azcatl, A.; Noh, J.; Madhvapathy, S. R.; Addou, R.; KC, S.; Dubey, M.; Cho, K.; Wallace, R. M.; Lee, S.-C.; He, J.-H.; Ager, J. W.; Zhang, X.; Yablonovitch, E.; Javey, A. Near-Unity Photoluminescence Quantum Yield in MoS<sub>2</sub>. *Science* (80-. ). **2015**, *350* (6264), 1065–1068. <https://doi.org/10.1126/science.aad2114>.
- (21) Lien, D. H.; Uddin, S. Z.; Yeh, M.; Amani, M.; Kim, H.; Ager, J. W.; Yablonovitch, E.;

- Javey, A. Electrical Suppression of All Nonradiative Recombination Pathways in Monolayer Semiconductors. *Science* (80-. ). **2019**, *364* (6439), 468–471. <https://doi.org/10.1126/science.aaw8053>.
- (22) Kim, H.; Uddin, S. Z.; Higashitarumizu, N.; Rabani, E.; Javey, A. Inhibited Nonradiative Decay at All Exciton Densities in Monolayer Semiconductors. *Science* (80-. ). **2021**, *373* (6553), 448–452. <https://doi.org/10.1126/science.abi9193>.
- (23) Amani, M.; Taheri, P.; Addou, R.; Ahn, G. H.; Kiriya, D.; Lien, D. H.; Ager, J. W.; Wallace, R. M.; Javey, A. Recombination Kinetics and Effects of Superacid Treatment in Sulfur- and Selenium-Based Transition Metal Dichalcogenides. *Nano Lett.* **2016**, *16* (4), 2786–2791. <https://doi.org/10.1021/acs.nanolett.6b00536>.
- (24) Goodman, A. J.; Lien, D. H.; Ahn, G. H.; Spiegel, L. L.; Amani, M.; Willard, A. P.; Javey, A.; Tisdale, W. A. Substrate-Dependent Exciton Diffusion and Annihilation in Chemically Treated MoS<sub>2</sub> and WS<sub>2</sub>. *J. Phys. Chem. C* **2020**, *124* (22), 12175–12184. <https://doi.org/10.1021/acs.jpcc.0c04000>.
- (25) Lee, Y.; Tran, T. T.; Kim, Y.; Roy, S.; Taniguchi, T.; Watanabe, K.; Jang, J. I.; Kim, J. Enhanced Radiative Exciton Recombination in Monolayer WS<sub>2</sub> on the hBN Substrate Competing with Nonradiative Exciton–Exciton Annihilation. *ACS Photonics* **2022**, *9* (3), 873–879. <https://doi.org/10.1021/acsp Photonics.1c01584>.
- (26) Kim, D.; Tran, T. T.; Taniguchi, T.; Watanabe, K.; Kim, J.; Jang, J. I. Temperature Dependence of Excitonic Auger Recombination in Excitonic-Complex-Free Monolayer WS<sub>2</sub> by Considering Auger Broadening and Generation Efficiency. *J. Phys. Chem. Lett.* **2023**, *14* (18), 4259–4265. <https://doi.org/10.1021/acs.jpcllett.3c00305>.
- (27) Lee, Y.; Kim, J. Controlling Lattice Defects and Inter-Exciton Interactions in Monolayer Transition Metal Dichalcogenides for Efficient Light Emission. *ACS Photonics* **2018**, *5* (11), 4187–4194. <https://doi.org/10.1021/acsp Photonics.8b00645>.

- (28) Lorchat, E.; López, L. E. P.; Robert, C.; Lagarde, D.; Froehlicher, G.; Taniguchi, T.; Watanabe, K.; Marie, X.; Berciaud, S. Filtering the Photoluminescence Spectra of Atomically Thin Semiconductors with Graphene. *Nat. Nanotechnol.* **2020**, *15* (4), 283–288. <https://doi.org/10.1038/s41565-020-0644-2>.
- (29) Lee, Y.; Ghimire, G.; Roy, S.; Kim, Y.; Seo, C.; Sood, A. K.; Jang, J. I.; Kim, J. Impeding Exciton-Exciton Annihilation in Monolayer WS<sub>2</sub> by Laser Irradiation. *ACS Photonics* **2018**, *5* (7), 2904–2911. <https://doi.org/10.1021/acsp Photonics.8b00249>.
- (30) Fu, Y.; He, D.; He, J.; Bian, A.; Zhang, L.; Liu, S.; Wang, Y.; Zhao, H. Effect of Dielectric Environment on Excitonic Dynamics in Monolayer WS<sub>2</sub>. *Adv. Mater. Interfaces* **2019**, *6* (23), 1901307. <https://doi.org/10.1002/admi.201901307>.
- (31) Liu, H.; Wang, C.; Liu, D.; Luo, J. Neutral and Defect-Induced Exciton Annihilation in Defective Monolayer WS<sub>2</sub>. *Nanoscale* **2019**, *11* (16), 7913–7920. <https://doi.org/10.1039/c9nr00967a>.
- (32) Zipfel, J.; Kulig, M.; Perea-Causín, R.; Brem, S.; Ziegler, J. D.; Rosati, R.; Taniguchi, T.; Watanabe, K.; Glazov, M. M.; Malic, E.; Chernikov, A. Exciton Diffusion in Monolayer Semiconductors with Suppressed Disorder. *Phys. Rev. B* **2020**, *101* (11), 115430. <https://doi.org/10.1103/PhysRevB.101.115430>.
- (33) Desai, S. B.; Seol, G.; Kang, J. S.; Fang, H.; Battaglia, C.; Kapadia, R.; Ager, J. W.; Guo, J.; Javey, A. Strain-Induced Indirect to Direct Bandgap Transition in Multilayer WSe<sub>2</sub>. *Nano Lett.* **2014**, *14* (8), 4592–4597. <https://doi.org/10.1021/nl501638a>.
- (34) Lee, Y.; Forte, J. D. S.; Chaves, A.; Kumar, A.; Tran, T. T.; Kim, Y.; Roy, S.; Taniguchi, T.; Watanabe, K.; Chernikov, A.; Jang, J. I.; Low, T.; Kim, J. Boosting Quantum Yields in Two-Dimensional Semiconductors via Proximal Metal Plates. *Nat. Commun.* **2021**, *12* (1), 7095. <https://doi.org/10.1038/s41467-021-27418-x>.
- (35) Uddin, S. Z.; Higashitarumizu, N.; Kim, H.; Rabani, E.; Javey, A. Engineering Exciton

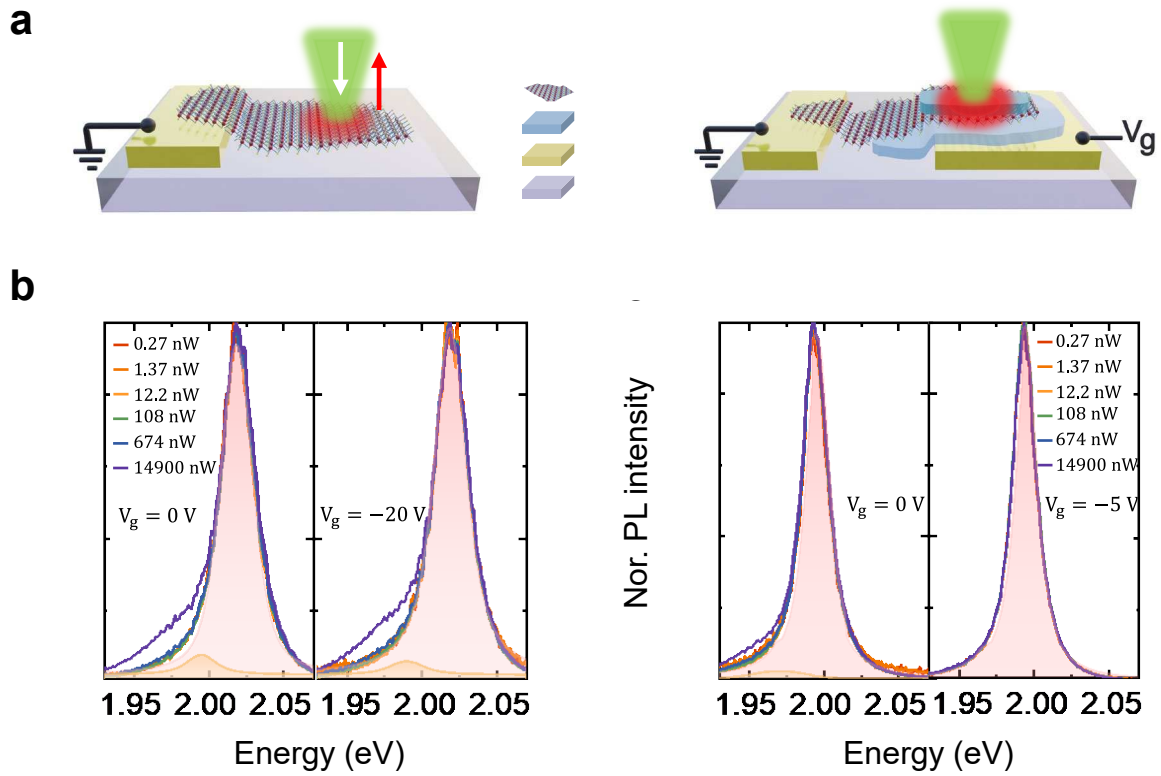
- Recombination Pathways in Bilayer WSe<sub>2</sub> for Bright Luminescence. *ACS Nano* **2022**, *16* (1), 1339–1345. <https://doi.org/10.1021/acsnano.1c09255>.
- (36) Strikha, M. V.; Kurchak, A. I.; Morozovska, A. N. Gate-Voltage Control of Quantum Yield in Monolayer Transition-Metal Dichalcogenide. *Phys. Rev. Appl.* **2020**, *13* (1), 014040. <https://doi.org/10.1103/PhysRevApplied.13.014040>.
- (37) Hu, Z.; Hernández-Martínez, P. L.; Liu, X.; Amara, M.-R.; Zhao, W.; Watanabe, K.; Taniguchi, T.; Demir, H. V.; Xiong, Q. Trion-Mediated Förster Resonance Energy Transfer and Optical Gating Effect in WS<sub>2</sub>/hBN/MoSe<sub>2</sub> Heterojunction. *ACS Nano* **2020**, *14* (10), 13470–13477. <https://doi.org/10.1021/acsnano.0c05447>.
- (38) Jauregui, L. A.; Joe, A. Y.; Pistunova, K.; Wild, D. S.; High, A. A.; Zhou, Y.; Scuri, G.; de Greve, K.; Sushko, A.; Yu, C. H.; Taniguchi, T.; Watanabe, K.; Needleman, D. J.; Lukin, M. D.; Park, H.; Kim, P. Electrical Control of Interlayer Exciton Dynamics in Atomically Thin Heterostructures. *Science* (80-. ). **2019**, *366* (6467), 870–875. <https://doi.org/10.1126/science.aaw4194>.
- (39) Barré, E.; Karni, O.; Liu, E.; O’Beirne, A. L.; Chen, X.; Ribeiro, H. B.; Yu, L.; Kim, B.; Watanabe, K.; Taniguchi, T.; Barmak, K.; Lui, C. H.; Refaely-Abramson, S.; da Jornada, F. H.; Heinz, T. F. Optical Absorption of Interlayer Excitons in Transition-Metal Dichalcogenide Heterostructures. *Science* (80-. ). **2022**, *376* (6591), 406–410. <https://doi.org/10.1126/science.abm8511>.
- (40) Sharma, A.; Zhu, Y.; Halbich, R.; Sun, X.; Zhang, L.; Wang, B.; Lu, Y. Engineering the Dynamics and Transport of Excitons, Trions, and Biexcitons in Monolayer WS<sub>2</sub>. *ACS Appl. Mater. Interfaces* **2022**, *14* (36), 41165–41177. <https://doi.org/10.1021/acсами.2c08199>.
- (41) Ross, J. S.; Wu, S.; Yu, H.; Ghimire, N. J.; Jones, A. M.; Aivazian, G.; Yan, J.; Mandrus, D. G.; Xiao, D.; Yao, W.; Xu, X. Electrical Control of Neutral and Charged Excitons in

- a Monolayer Semiconductor. *Nat. Commun.* **2013**, *4* (1), 1474.  
<https://doi.org/10.1038/ncomms2498>.
- (42) Moody, G.; Schaibley, J.; Xu, X. Exciton Dynamics in Monolayer Transition Metal Dichalcogenides. *J. Opt. Soc. Am. B* **2016**, *33* (7), C39.  
<https://doi.org/10.1364/JOSAB.33.000C39>.
- (43) Cadiz, F.; Courtade, E.; Robert, C.; Wang, G.; Shen, Y.; Cai, H.; Taniguchi, T.; Watanabe, K.; Carrere, H.; Lagarde, D.; Manca, M.; Amand, T.; Renucci, P.; Tongay, S.; Marie, X.; Urbaszek, B. Excitonic Linewidth Approaching the Homogeneous Limit in MoS<sub>2</sub>-Based van Der Waals Heterostructures. *Phys. Rev. X* **2017**, *7* (2), 1–12.  
<https://doi.org/10.1103/PhysRevX.7.021026>.
- (44) Grzeszczyk, M.; Olkowska-Pucko, K.; Nogajewski, K.; Watanabe, K.; Taniguchi, T.; Kossacki, P.; Babiński, A.; Molas, M. R. Exposing the Trion's Fine Structure by Controlling the Carrier Concentration in hBN-Encapsulated MoS<sub>2</sub>. *Nanoscale* **2021**, *13* (44), 18726–18733. <https://doi.org/10.1039/d1nr03855a>.
- (45) Kajino, Y.; Oto, K.; Yamada, Y. Modification of Optical Properties in Monolayer WS<sub>2</sub> on Dielectric Substrates by Coulomb Engineering. *J. Phys. Chem. C* **2019**, *123* (22), 14097–14102. <https://doi.org/10.1021/acs.jpcc.9b04514>.
- (46) McCreary, K. M.; Hanbicki, A. T.; Singh, S.; Kawakami, R. K.; Jernigan, G. G.; Ishigami, M.; Ng, A.; Brintlinger, T. H.; Stroud, R. M.; Jonker, B. T. The Effect of Preparation Conditions on Raman and Photoluminescence of Monolayer WS<sub>2</sub>. *Sci. Rep.* **2016**, *6* (1), 35154. <https://doi.org/10.1038/srep35154>.
- (47) Ding, L.; Ukhtary, M. S.; Chubarov, M.; Choudhury, T. H.; Zhang, F.; Yang, R.; Zhang, A.; Fan, J. A.; Terrones, M.; Redwing, J. M.; Yang, T.; Li, M.; Saito, R.; Huang, S. Understanding Interlayer Coupling in TMD-hBN Heterostructure by Raman Spectroscopy. *IEEE Trans. Electron Devices* **2018**, *65* (10), 4059–4067.

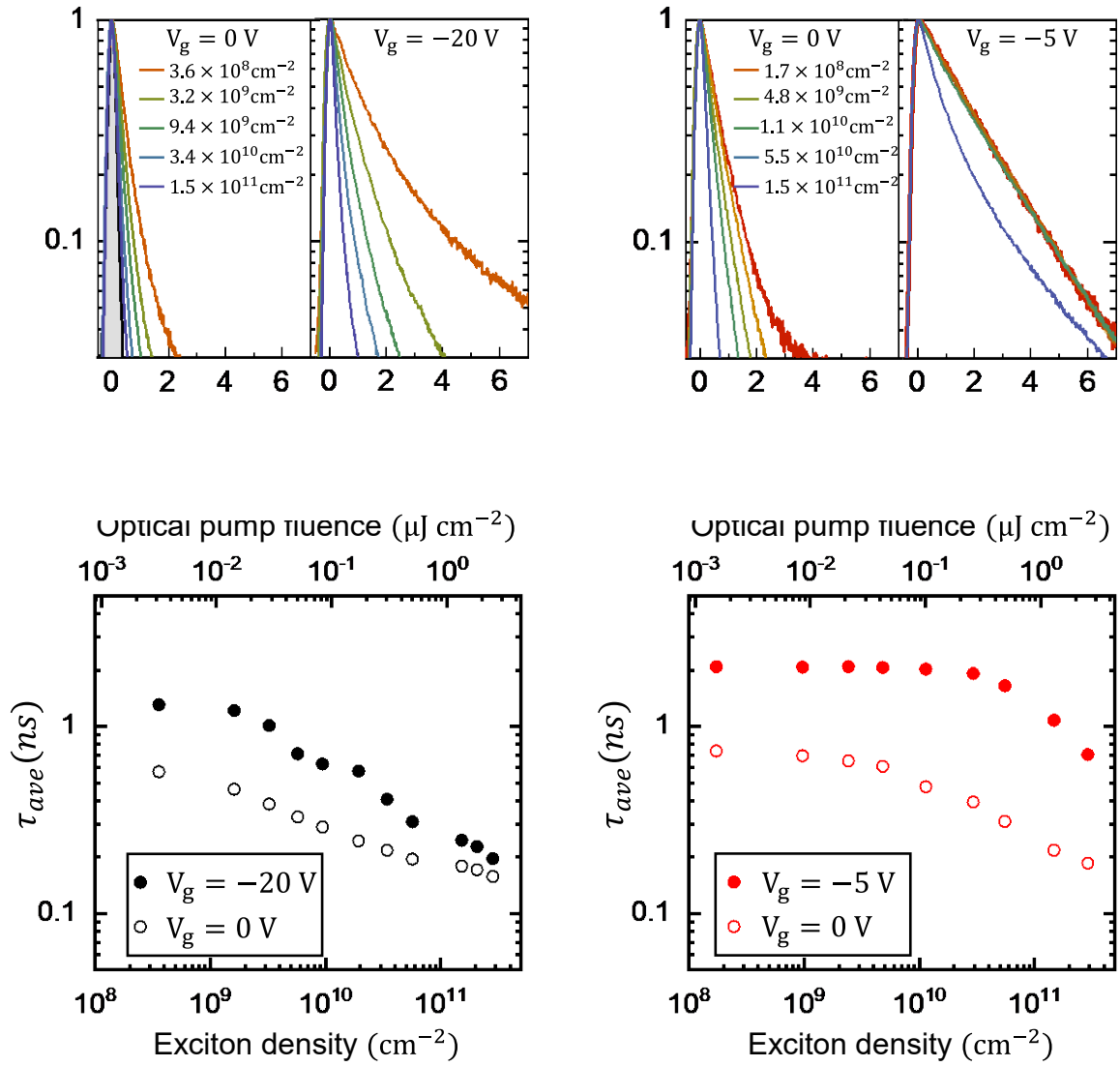
- <https://doi.org/10.1109/TED.2018.2847230>.
- (48) Buscema, M.; Steele, G. A.; van der Zant, H. S. J.; Castellanos-Gomez, A. The Effect of the Substrate on the Raman and Photoluminescence Emission of Single-Layer MoS<sub>2</sub>. *Nano Res.* **2014**, *7* (4), 561–571. <https://doi.org/10.1007/s12274-014-0424-0>.
- (49) Mouri, S.; Miyauchi, Y.; Toh, M.; Zhao, W.; Eda, G.; Matsuda, K. Nonlinear Photoluminescence in Atomically Thin Layered WSe<sub>2</sub> Arising from Diffusion-Assisted Exciton-Exciton Annihilation. *Phys. Rev. B* **2014**, *90* (15), 155449. <https://doi.org/10.1103/PhysRevB.90.155449>.
- (50) Hoshi, Y.; Kuroda, T.; Okada, M.; Moriya, R.; Masubuchi, S.; Watanabe, K.; Taniguchi, T.; Kitaura, R.; Machida, T. Suppression of Exciton-Exciton Annihilation in Tungsten Disulfide Monolayers Encapsulated by Hexagonal Boron Nitrides. *Phys. Rev. B* **2017**, *95* (24), 241403. <https://doi.org/10.1103/PhysRevB.95.241403>.
- (51) Yuan, L.; Wang, T.; Zhu, T.; Zhou, M.; Huang, L. Exciton Dynamics, Transport, and Annihilation in Atomically Thin Two-Dimensional Semiconductors. *J. Phys. Chem. Lett.* **2017**, *8* (14), 3371–3379. <https://doi.org/10.1021/acs.jpcclett.7b00885>.
- (52) Jo, S.; Ubrig, N.; Berger, H.; Kuzmenko, A. B.; Morpurgo, A. F. Mono- and Bilayer WS<sub>2</sub> Light-Emitting Transistors. *Nano Lett.* **2014**, *14* (4), 2019–2025. <https://doi.org/10.1021/nl500171v>.
- (53) Alharbi, A.; Shahrjerdi, D. Electronic Properties of Monolayer Tungsten Disulfide Grown by Chemical Vapor Deposition. *Appl. Phys. Lett.* **2016**, *109* (19), 193502. <https://doi.org/10.1063/1.4967188>.
- (54) Liu, Y.; Stradins, P.; Wei, S. H. Van Der Waals Metal-Semiconductor Junction: Weak Fermi Level Pinning Enables Effective Tuning of Schottky Barrier. *Sci. Adv.* **2016**, *2* (4), 1–7. <https://doi.org/10.1126/sciadv.1600069>.
- (55) Nagler, P.; Plechinger, G.; Ballottin, M. V.; Mitioglu, A.; Meier, S.; Paradiso, N.; Strunk,

- C.; Chernikov, A.; Christianen, P. C. M.; Schüller, C.; Korn, T. Interlayer Exciton Dynamics in a Dichalcogenide Monolayer Heterostructure. *2D Mater.* **2017**, *4* (2), 025112. <https://doi.org/10.1088/2053-1583/aa7352>.
- (56) Ovchinnikov, D.; Allain, A.; Huang, Y.-S.; Dumcenco, D.; Kis, A. Electrical Transport Properties of Single-Layer WS<sub>2</sub>. *ACS Nano* **2014**, *8* (8), 8174–8181. <https://doi.org/10.1021/nm502362b>.
- (57) Wang, H.; Strait, J. H.; Zhang, C.; Chan, W.; Manolatou, C.; Tiwari, S.; Rana, F. Fast Exciton Annihilation by Capture of Electrons or Holes by Defects via Auger Scattering in Monolayer Metal Dichalcogenides. *Phys. Rev. B* **2015**, *91* (16), 165411. <https://doi.org/10.1103/PhysRevB.91.165411>.
- (58) Cavalcante, L. S. R.; Chaves, A.; Van Duppen, B.; Peeters, F. M.; Reichman, D. R. Electrostatics of Electron-Hole Interactions in van Der Waals Heterostructures. *Phys. Rev. B* **2018**, *97* (12), 125427. <https://doi.org/10.1103/PhysRevB.97.125427>.
- (59) Robert, C.; Lagarde, D.; Cadiz, F.; Wang, G.; Lassagne, B.; Amand, T.; Balocchi, A.; Renucci, P.; Tongay, S.; Urbaszek, B.; Marie, X. Exciton Radiative Lifetime in Transition Metal Dichalcogenide Monolayers. *Phys. Rev. B* **2016**, *93* (20), 205423. <https://doi.org/10.1103/PhysRevB.93.205423>.
- (60) Peimyoo, N.; Yang, W.; Shang, J.; Shen, X.; Wang, Y.; Yu, T. Chemically Driven Tunable Light Emission of Charged and Neutral Excitons in Monolayer WS<sub>2</sub>. *ACS Nano* **2014**, *8* (11), 11320–11329. <https://doi.org/10.1021/nm504196n>.
- (61) Wan, Y.; Li, E.; Yu, Z.; Huang, J.-K.; Li, M.-Y.; Chou, A.-S.; Lee, Y.-T.; Lee, C.-J.; Hsu, H.-C.; Zhan, Q.; Aljarb, A.; Fu, J.-H.; Chiu, S.-P.; Wang, X.; Lin, J.-J.; Chiu, Y.-P.; Chang, W.-H.; Wang, H.; Shi, Y.; Lin, N.; Cheng, Y.; Tung, V.; Li, L.-J. Low-Defect-Density WS<sub>2</sub> by Hydroxide Vapor Phase Deposition. *Nat. Commun.* **2022**, *13* (1), 4149. <https://doi.org/10.1038/s41467-022-31886-0>.

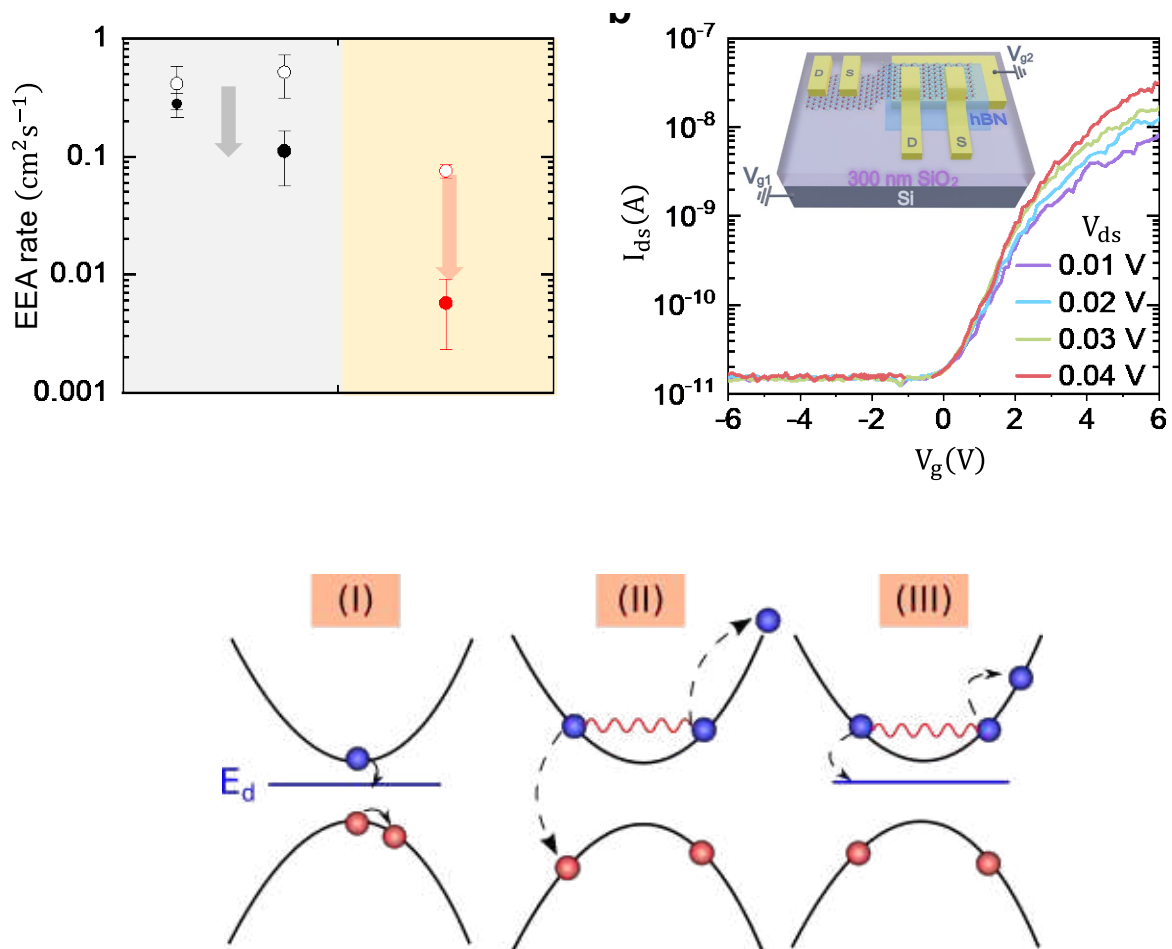
- (62) Pradeepa, H. L.; Mondal, P.; Bid, A.; Basu, J. K. Electrical and Chemical Tuning of Exciton Lifetime in Monolayer MoS<sub>2</sub> for Field-Effect Transistors. *ACS Appl. Nano Mater.* **2020**, *3* (1), 641–647. <https://doi.org/10.1021/acsanm.9b02170>.
- (63) Rigosi, A. F.; Hill, H. M.; Li, Y.; Chernikov, A.; Heinz, T. F. Probing Interlayer Interactions in Transition Metal Dichalcogenide Heterostructures by Optical Spectroscopy: MoS<sub>2</sub>/WS<sub>2</sub> and MoSe<sub>2</sub>/WSe<sub>2</sub>. *Nano Lett.* **2015**, *15* (8), 5033–5038. <https://doi.org/10.1021/acs.nanolett.5b01055>.
- (64) Castellanos-Gomez, A.; Buscema, M.; Molenaar, R.; Singh, V.; Janssen, L.; van der Zant, H. S. J.; Steele, G. A. Deterministic Transfer of Two-Dimensional Materials by All-Dry Viscoelastic Stamping. *2D Mater.* **2013**, *1* (1), 011002. <https://doi.org/10.1088/2053-1583/1/1/011002>.



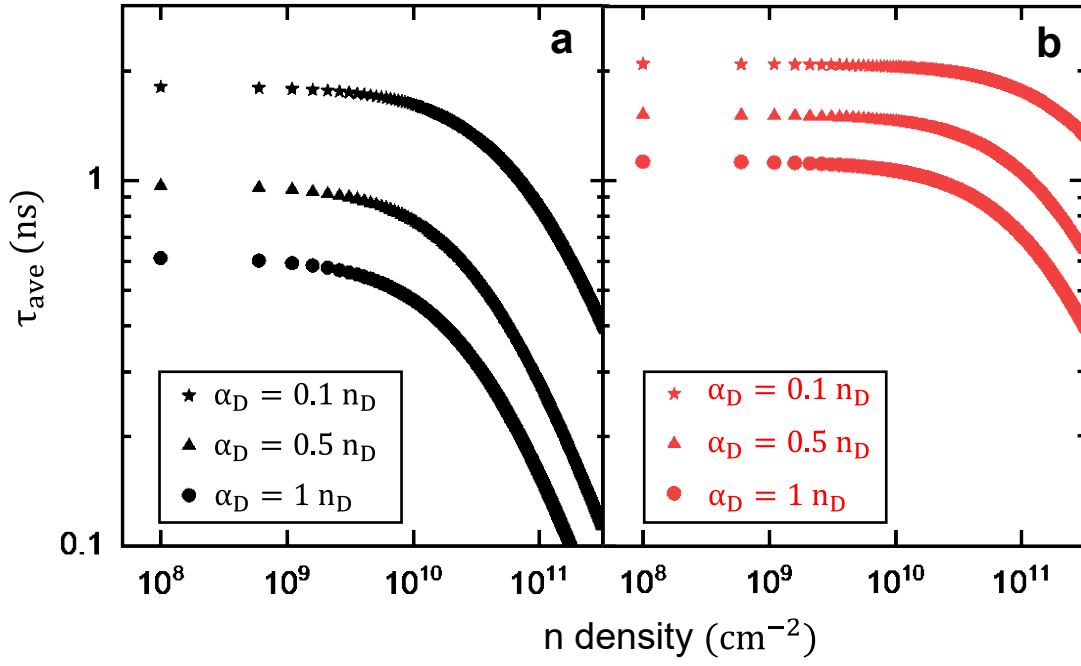
**Figure 1.** Sample configurations and normalized PL of 1L-WS<sub>2</sub> under NEGB ( $V_g$ ). (a) Schematics for the device structures of Sample A (left panel) and Sample B (right panel).  $V_g$  is  $-20$  V and  $-5$  V for the former and the latter, respectively. Normalized (Nor.) PL spectra of 1L-WS<sub>2</sub> under varying excitation powers from 0.27 to 14900 nW for (b) Sample A and (c) Sample B. Deconvolution of the PL peaks into excitons and trions are indicated with the shadows in pink and orange, respectively. Excitation powers are indicated in the legend, and the right panel and the left panel are with and without  $V_g$ , respectively.



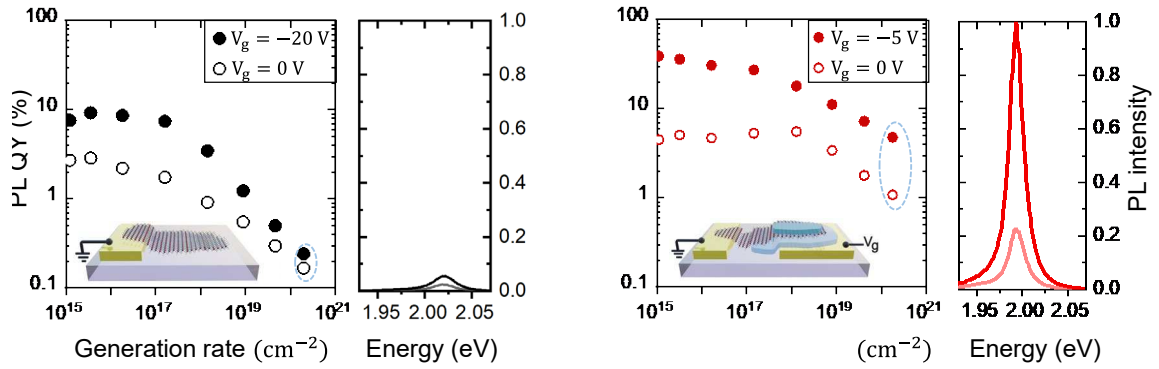
**Figure 2.** Variation of PL lifetimes of 1L-WS<sub>2</sub> at different initial exciton densities from **(a)** Sample A and **(b)** Sample B. The initial exciton density,  $n_{ex}(0)$ , is indicated in the legend. The right (left) panel is with (without) NEGB. The IRF is shown as the grey shaded curve in the left panel in (a) and is identical for other sample configurations. Plots of PL lifetime ( $\tau_{ave}$  vs. exciton density) of **(c)** Sample A and **(d)** Sample B with (solid dots) and without (open circles)  $V_g$ .



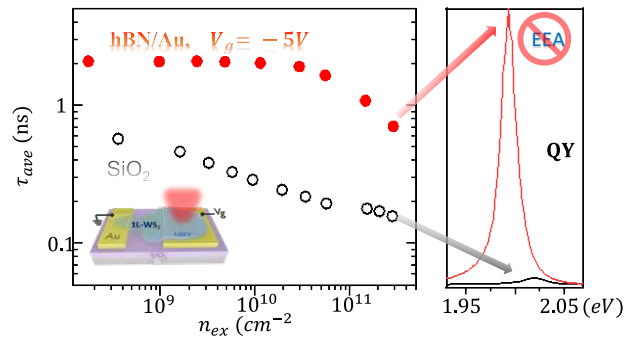
**Figure 3.** Estimated EEA rate constants of 1L-WS<sub>2</sub> in various sample configurations. **(a)** EEA rates of Sample A (black) and Sample B (red) without (open circles) and with bias (solid dots). Error bars represent the standard deviations from the measurements of multiple samples. **(b)** Transfer characteristics ( $I_{ds}$  vs.  $V_g$ ) of the 1L-WS<sub>2</sub> FET on the hBN/Au substrate. Inset is the schematic of the FET device. **(c)** Nonradiative decay channels for excitons; process I is defect-assisted exciton recombination, process II is EEA, and process III is defect-assisted EEA, respectively.



**Figure 4.** Theoretical estimation of the average PL lifetime  $\tau_{ave}$  as a function of the initial exciton density  $n_{ex}(0)$  of 1L-WS $_2$  on **(a)** SiO $_2$ , and **(b)** 8-nm-thick hBN on the Au substrate, assuming two fractional values of active defects  $\alpha_D$ . The defect density is assumed to be  $n_D = 5 \times 10^{12}$  cm $^{-2}$ .



**Figure 5.** Left panels: Plot of PL QY vs. exciton generation rate from **(a)** Sample A and **(b)** Sample B. Open circles and solid dots represent the data obtained without and with NEGB. Insets are schematics of sample configurations. Right panels: Selected PL spectra (dotted ellipsoids in PL QY plots) with the relative peak intensities normalized to the PL QY values of Sample B with NEGB.



For Table of Contents Only